Angular measurements of light scattered by turbid chiral media using linear Stokes polarimeter

Xinxin Guo
Michael F. G. Wood
Ontario Cancer Institute
Division of Biophysics and Bioimaging
and
University of Toronto
Department of Medical Biophysics
610 University Avenue
Toronto, Ontario M5G 2M9
Canada

I. Alex Vitkin
Ontario Cancer Institute
Division of Biophysics and Bioimaging
and
University of Toronto
Departments of Medical Biophysics and
Radiation Oncology
610 University Avenue
Toronto, Ontario M5G 2M9
Canada
E-mail: vitkin@uhnres.utoronto.ca

Abstract. The effects of turbid chiral media on light polarization are studied in different directions around the scattering samples using a refined linear Stokes polarimeter, which simplifies the signal analysis, and allows for the detailed investigations of scattered light. Because no moving parts are involved in a measurement at a specific detection direction, the determination accuracy of polarization states is increased. The results show that light depolarization increases with both turbidity and detection angle for low and moderately turbid samples; however, the angular dependence decreases with increasing turbidity. When the turbidity is increased to $\sim 100\ \mathrm{cm}^{-1}$, the depolarization becomes higher in the forward than in the backward direction. Polarization sensitive Monte Carlo simulations are used to verify some experimental observations. The results also demonstrate that surviving linear polarization fraction and overall intensity are more sensitive to the increase of glucose concentration in backward than in the forward direction in highly turbid media, indicating that backward geometry may be preferable for potential glucose detection in a biomedical context. Comparison measurements with optically inactive glycerol suggest that the refractive index matching effect, and not the chiral nature of the solute, dominates the observed optical rotation engendered by glucose in highly turbid media. [DOI: 10.1117/1.2339134]

Keywords: optical polarization; turbid polarimetry; glucose detection; multiple scattering; Monte Carlo simulations; linear Stokes polarimeter.

Paper 05246SSR received Aug. 22, 2005; revised manuscript received Jan. 16, 2006; accepted for publication May 12, 2006; published online Sep. 1, 2006.

1 Introduction

Diabetes mellitus is a medical condition in which the body cannot adequately produce or effectively use insulin that is needed to maintain a normal blood glucose level. It is reported that diabetes afflicts over 15 million people in North America and 100 million people worldwide.[1] To avoid or to delay the complication of diabetes including blindness, heart disease, and kidney failure, diabetics must regulate their insulin injections and caloric intake by monitoring their blood glucose levels. Most current methods for glucose monitoring require drawing blood (typically via a finger prick), which is painful, inconvenient, potentially infectious, and otherwise suboptimal. Significant efforts have centered on the search for noninvasive glucose monitoring methods. Optical methods are potentially well-suited to tackle this currently unsolved problem due to their noninvasive, nonharmful nature and sensitivity to glucose-induced optical changes.[2–10]

Recently, polarized light has been used to extract quantitative information from the optically thick tissues with which it interacts.[3,10–15] Because the optics of skin is dominated by scattering effects in the tissue optical window range of 600 to 1200 nm, the understanding of polarization properties of light that has escaped from highly scattering media is of great importance. In addition to the forward direction, some research has examined the detection of scattered light in other directions,[11–13] to investigate the detection geometry where the experimental observables such as optical rotation, degree of polarization, and intensity respond most to changes in glucose concentration. These attempts were challenged by the complexity of light-media interactions and experimental difficulties.[12–15]

The approach presented in this paper employs a refined linear Stokes polarimeter to detect the emerging light polarization states in a variety of detection angles around a scattering sample and examines the sensitivity of the derived changes in optical rotation and surviving linear polarization fraction to changes in the glucose concentration. This polarimeter design is similar to the one presented by Hunt and Huffman in the 1970s and subsequently used by many researchers.[16–19] The main innovation in the present embodiment lies in the measurement of various harmonics of the signal, which are *directly* related to the linear Stokes vector components of the sample-scattered light. In other words, the current arrangement with the polarization modulation in the analyzer arm after the sample, permits completely

Address all correspondence to I. Alex Vitkin, University of Toronto, Department of Medical Biophysics, Princess Margaret Hospital, 610 University Ave, Toronto, Ontario MSG 2M9, Canada; Tel: 416 946 4501 Ext. 5742; Fax: 416 946 6529; E-mail: vitkin@uhnres.utoronto.ca

1083-3668/2006/11(4)/041105/10/$22.00

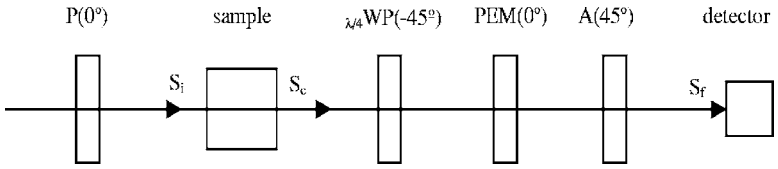

Fig. 1 Simplified linear Stokes polarimeter set-up. P, polarizer; A, analyzer; WP, quarter wave plate; PEM, photoelastic modulator; S_i, Stokes vector of the incident beam; S_e, Stokes vector of the emerging beam; S_f, Stokes vector of the beam reaching detector. All angles are with respect to the optical table.

assumption-independent determination of sample-induced light polarization parameters. This is a significant improvement over many previous attempts at Mueller matrix or Stokes vector polarimetry, which had to assume specific forms of the sample matrix or of the scattered light components for signal analysis. These assumptions become questionable as one encounters complicated media, such as biological tissues, that may exhibit several optically active effects at once (linear and circular birefringence or dichroism) while also causing light depolarization due to multiple scattering. Also, the electronic synchronous detection at three different modulation frequencies provides sufficient information to determine the Stokes parameters of interest, without the need for mechanical moving parts (rotating linear polarizers and/or wave plates, swapping in and out of polarizing optics). This reduces noise in the polarization measurements. Utilizing the linear Stokes polarimeter, the relative contributions of glucose concentration, sample turbidity, and detection angle geometry to the polarization properties of the emerging light are systematically investigated. The role of optical activity of glucose, the foundation for glucometry in clear and low turbid media, in the observed optical rotation in highly turbid media is also investigated.

2 Theory and Signal Analysis

2.1 *Theory*

Figure 1 illustrates the simplified linear Stokes polarimeter setup. The approach is centered on polarization modulation accomplished by the photoelastic modulator (PEM) and synchronous detection via a lock-in amplifier, allowing a sensitive means of detecting low levels of polarization signals in the presence of largely depolarized background. Specifically, the laser beam passes through a linear polarizer P (pass axis horizontal, parallel to the optical table) and impinges on the sample. The scattered light from the sample passes through a quarter wave plate, whose fast-axis orientation is −45° with respect to optical table, and goes through the PEM block orientated horizontally. The PEM is a resonant device operating at 50 kHz whose user-defined peak retardance δ_0 is selected to optimize polarization signal strength (see below). The light then passes through an analyzer A set at 45° with respect to the optical table and finally reaches the detector. Using standard Stokes vector notation for light polarization and Mueller matrices to represent the optical elements that transform these polarization states, we now analyze the system in Fig. 1. $\mathbf{S}_i$ represents the Stokes vector of the incident beam

$$\mathbf{S}_i = [1 \quad 1 \quad 0 \quad 0]^T, \tag{1}$$

where horizontal notation is used for convenience, with T standing for the transpose of the vector. $\mathbf{S}_e$ is the Stokes vector of the emerging beam after sample interactions,

$$\mathbf{S}_e = [I \quad Q \quad U \quad V]^T. \tag{2}$$

If the elements of the Stokes vector in Eq. (2) are normalized by intensity I, Eq. (2) becomes

$$\mathbf{S}_e = I[1 \quad q \quad u \quad v]^T, \tag{3}$$

where $q=\frac{Q}{I}$, $u=\frac{U}{I}$, and $v=\frac{V}{I}$. $\mathbf{S}_f$ is the Stokes vector of the beam reaching the detector

$$\mathbf{S}_f = [I_f \quad Q_f \quad U_f \quad V_f]^T. \tag{4}$$

Relating the detected signal to the sample-emerging beam via Mueller calculus,

$$\mathbf{S}_f = \mathbf{M}_A \mathbf{M}_{PEM} \mathbf{M}_{WP} \mathbf{S}_e, \tag{5}$$

where $\mathbf{M}_{WP}$ is the Mueller matrix of the quarter wave plate, $\mathbf{M}_{PEM}$ is the Mueller matrix of the PEM, and $\mathbf{M}_A$ is the Mueller matrix of the analyzer. For the selected orientations, the Mueller matrices are

$$\mathbf{M}_{WP}(-45^\circ) = \begin{bmatrix} 1 & 0 & 0 & 0 \\ 0 & 0 & 0 & 1 \\ 0 & 0 & 1 & 0 \\ 0 & -1 & 0 & 0 \end{bmatrix}, \tag{6}$$

$$\mathbf{M}_{PEM}(0^\circ) = \begin{bmatrix} 1 & 0 & 0 & 0 \\ 0 & 1 & 0 & 0 \\ 0 & 0 & \cos\delta & \sin\delta \\ 0 & 0 & -\sin\delta & \cos\delta \end{bmatrix}, \tag{7}$$

$$\mathbf{M}_A(45^\circ) = \frac{1}{2}\begin{bmatrix} 1 & 0 & 1 & 0 \\ 0 & 0 & 0 & 0 \\ 1 & 0 & 1 & 0 \\ 0 & 0 & 0 & 0 \end{bmatrix}. \tag{8}$$

Putting Eqs. (6)–(8) and (3) into Eq. (5), we obtain

$$\mathbf{S}_f = \frac{1}{2}\begin{bmatrix} 1 & 0 & 1 & 0 \\ 0 & 0 & 0 & 0 \\ 1 & 0 & 1 & 0 \\ 0 & 0 & 0 & 0 \end{bmatrix}\begin{bmatrix} 1 & 0 & 1 & 0 \\ 0 & 1 & 0 & 0 \\ 0 & 0 & \cos\delta & \sin\delta \\ 0 & 0 & -\sin\delta & \cos\delta \end{bmatrix} \times \begin{bmatrix} 1 & 0 & 0 & 0 \\ 0 & 0 & 0 & 1 \\ 0 & 0 & 1 & 0 \\ 0 & -1 & 0 & 0 \end{bmatrix}\begin{bmatrix} 1 \\ q \\ u \\ v \end{bmatrix}. \quad (9)$$

Performing the multiplications, the measurable part of the final Stokes vector reaching the detector is the time-dependent intensity expressed as

$$I_f(t) = \frac{1}{2}[1 - q\sin\delta + u\cos\delta] = \frac{I}{2}[1 - q\sin(\delta_0\sin\omega t) + u\cos(\delta_0\sin\omega t)], \quad (10)$$

where the time-dependent PEM retardation follows $\delta(t) = \delta_0\sin(\omega t)$. Applying Fourier expansion in terms of Bessel functions

$$\sin\delta = \sin(\delta_0\sin\omega t) = 2\sum_{n=1}^{\infty} J_{2n-1}(\delta_0)\sin(2n-1)\omega t, \quad (11)$$

$$\cos\delta = \cos(\delta_0\sin\omega t) = \mathrm{J}_0(\delta_0) + 2\sum_{n=1}^{\infty} J_{2n}(\delta_0)\cos 2n\omega t, \quad (12)$$

to sine and cosine terms in Eq. (10), there results

$$I_f(t) = \frac{1}{2}\{1 - 2J_1(\delta_0)q\sin\omega t + u[J_0(\delta_0) + J_2(\delta_0)\cos 2\omega t] + \cdots\}. \quad (13)$$

If the peak retardance of PEM is set to $\delta_0 = 2.405$ radians so that $J_0(\delta_0) = 0$, then

$$I_f(t) = \frac{1}{2}[1 - 2J_1(\delta_0)q\sin\omega t + 2J_2(\delta_0)u\cos 2\omega t + \cdots]. \quad (14)$$

The elements of the Stokes vector of the sample-scattered light, I, q, and u [Eq. (3)] can be extracted from the dc component, first harmonic component, and second harmonic component of Eq. (14), respectively. Equation (14) is valid for all scattering directions because no angle-dependent assumptions are used in its derivation. Further, this formulation is based on the general form of sample polarization in Eq. (3), thus avoiding the assumption of specific (and generally unknown) forms of the sample Mueller matrix that may simultaneously exhibit optical rotation, depolarization, and linear anisotropy (birefringence).[12,14] As such, the relationship of the derived polarization parameters to the intrinsic properties of the interrogated sample is further strengthened.

2.2 *Signal Analysis*

If the dc component of Eq. (14) is measured by an electronic dc voltmeter, and the first and second harmonic components are measured by a lock-in amplifier, the experimentally observed wave form will be

$$V(t) = V_{DC} + \sqrt{2}V_{1f}\sin(\omega t) + \sqrt{2}V_{2f}\cos(2\omega t), \quad (15)$$

where V_{DC} is the dc measurement in volts, V_{1f} is lock-in output in volts (rms) at the PEM's first harmonic, and V_{2f} is lock-in output in volts (rms) at the PEM's second harmonic. The factor $\sqrt{2}$ arises in Eq. (15) because the lock-in amplifier reports rms voltage.

By comparing Eq. (14) with Eq. (15),

$$V_{DC} = \frac{I}{2}k, \quad (16)$$

$$\sqrt{2}V_{1f} = -IkJ_1(\delta_0)q, \quad (17)$$

$$\sqrt{2}V_{2f} = -IkJ_2(\delta_0)u, \quad (18)$$

where k is an instrumental constant, the same for all three equations assuming constant detector frequency response. Equations (16)–(18) yield expressions for q and u in terms of the experimentally measured parameters

$$q = \frac{-1}{\sqrt{2}J_1(\delta_0)}\frac{V_{1f}}{V_{DC}}, \quad (19)$$

$$u = \frac{1}{\sqrt{2}J_2(\delta_0)}\frac{V_{2f}}{V_{DC}}. \quad (20)$$

The optical rotation of the emerging beam α and surviving linear polarization fraction β_{linear} can be calculated accordingly

$$\alpha = \frac{1}{2}\tan^{-1}\left(\frac{U}{Q}\right) = \frac{1}{2}\tan^{-1}\left(\frac{u}{q}\right), \quad (21)$$

$$\beta_{linear} = \frac{\sqrt{Q^2 + U^2}}{I} = \sqrt{q^2 + u^2}. \quad (22)$$

Strictly speaking, α is the orientation of polarization ellipse of the emerging beam, but can be treated as the optical rotation with reference to the orientation of the polarization ellipse of the incident beam expressed in Eq. (1). In order to increase dc measurement accuracy, for example, to eliminate the effects of light intensity fluctuation, it is useful to employ ac methods based on lock-in amplification. This is convenient in the current set-up that already uses lock-in detection for the PEM-based signals and will ensure the cancellation of the experimentally unknown constant factor k that is needed for the correct derivations of Eqs. (16)–(20). If we use a mechanical "square wave" chopper with a duty cycle of 50%, the average

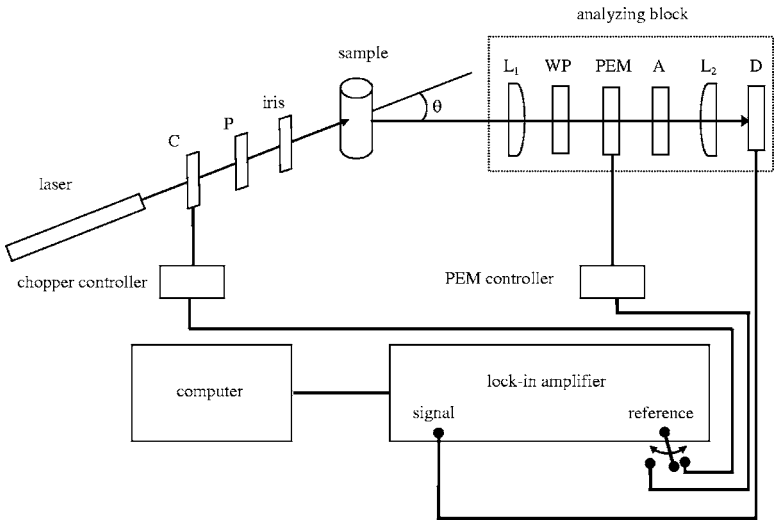

Fig. 2 Schematic diagram of linear Stokes polarimeter. C, optical chopper; P, polarizer; θ, detection angle; L_1 and L_2, plano-convex lenses; WP, quarter wave plate; PEM, photoelastic modulator; A, analyzer; D, detector.

dc, $1f$ and $2f$ signal intensities will all be halved, and the ratios of V_{AC}/V_{DC} will remain unchanged. However, the lock-in output of dc measurement $V_{chopper}$ is not precisely the V_{DC} value. The relationship between the chopper signal measured by the lock-in amplifier $V_{chopper}$ and V_{DC} is

$$V_{DC} = 1.1107 V_{chopper}, \tag{23}$$

which has universal validity for square wave choppers with 50% duty cycle.[20] In Eqs. (19) and (20), replacing V_{DC} with Eq. (23) and using $J_1(\delta_0)=0.51911$ and $J_2(\delta_0)=0.43169$, we get

$$q = \frac{-1}{\sqrt{2} \times 0.51911 \times 1.1107} \frac{V_{1f}}{V_{chopper}}, \tag{24}$$

$$u = \frac{1}{\sqrt{2} \times 0.43169 \times 1.1107} \frac{V_{2f}}{V_{chopper}}. \tag{25}$$

Equations (24) and (25) yield the sample Stokes parameters from data acquired only by synchronous high signal-to-noise ratio lock-in amplifier detection, which in turn yield accurate estimates of sample-induced optical rotations α and linear polarization fraction β_{linear} via Eqs. (21) and (22).

3 Materials and Experiments

3.1 *Experiment Setup*

Figure 2 shows the diagram of linear Stokes polarimeter, demonstrating the specific embodiment of the general set-up of Fig. 1. The 632.8-nm light from a HeNe laser (Research Electro-Optics, LHRR-120M), chopped by a mechanical chopper at a frequency of 500 Hz, passes through a polarizer (pass axis horizontal) and an iris of 1 mm diameter, and strikes a round glass cuvette of 1 cm inner diameter that contains the sample. For the reported experiments, the effective sampling volume is a function of detection geometry and sample scattering properties. Its approximate range varies from a few cubic millimeters (highly scattering, large detection angles) to tens of cubic millimeters. Further quantification of this important but difficult parameter, and a related measure we call the average photon pathlength, will be reported in a forthcoming publication. The incident power on the sample is ~1 mW. Part of the emerging light enters an analyzing block consisting of a pair of plano-convex lenses; a quarter wave plate (fast axis at −45°); a PEM (Hinds Instruments IS-90; horizontal retardation axis, oscillating at 50 kHz), a linear analyzer (pass axis at +45°), and a polarization-insensitive avalanche photodiode detector (Hamamatsu, C5460), which has a flat frequency response range from dc to 1 MHz. The analyzing block is installed on a horizontally rotatable platform forming a detection angle θ with respect to the incident light, with the center of the cylindrical cuvette positioned at the rotation axis of the block. The use of the pair of plano-convex lenses increases measurement sensitivity. The first lens picks up emerging light from an area of the turbid sample that is small enough to avoid significant blurring of the polarization states engendered by spatial averaging. The collected light is then converted into a collimated beam by the lens, an important step as the PEM functions optimally with collimated light. The second lens converges the collimated light, focusing it onto the sensing area of the detector. The signal from the analyzing block is sent to a lock-in amplifier (Standford Research Systems, SR830). The reference input of the lock-in amplifier is toggled between the chopper and PEM controllers. Data acquisition is carried out under computer control, obtaining within 2 min 10-measurement averages at 500 Hz, 50 kHz, and 100 kHz as $V_{chopper}$, V_{1f}, and V_{2f} for further processing. The detection angle scanning is achieved by rotating the analyzing block platform as it isocentrically pivots around the round cuvette. The angles in the experiment vary from 0 to 155° at 5° intervals. Because of the PEM's size ($15 \times 2.5 \times 5.5$ cm^3), the measurements at angles larger than $\theta > 155°$ are hindered due to the obstruction of incident beam by the analyzing block.

3.2 *Materials*

Four sets of samples were used in the experiments. The first set consists of turbid media with different scattering coefficients. These are suspensions of polystyrene microspheres (refractive index $n_s=1.59$, density $\rho=1.05\ \mathrm{g/cm^3}$, radius $r=0.7\ \mu\mathrm{m}$), yielding a scattering efficiency of $Q_{sca}=3.56$ at $\lambda=632.8$ nm in deionized water.[21] The weight fraction of microspheres f_w ranges from 5.5×10^{-4} to 2.7×10^{-3}. Because scattering coefficient μ_s is equal to the product of the scattering cross-section $\sigma_{sca}=Q_{sca}\pi r^2$ and the scatterer volume density $\rho_{sca}f_v/[(4/3)\pi r^3]$ (f_v is the volume fraction of the scatterers), $\mu_s=\{f_v/[(4/3)\pi r^3]\}Q_{sca}\pi r^2=3Q_{sca}f_w\rho_0/4r\rho$ [ρ_0 is the water density ($1\ \mathrm{g/cm^3}$)], the corresponding scattering coefficients vary from 20 to 100 $\mathrm{cm^{-1}}$. The second set of samples are turbid media containing *D*-glucose with the microsphere weight fraction kept constant at 8.25×10^{-4} (μ_s is ~27.8 to 30 $\mathrm{cm^{-1}}$, depending on glucose levels) and glucose concentration ranging from 20 to 900 mM. The third set of samples are highly turbid media containing *D*-glucose with the microsphere weight fraction kept constant at 2.75×10^{-3} (μ_s is ~92.75 to 99.9 $\mathrm{cm^{-1}}$, depending on glucose levels) and glucose concentration ranging from 30 to 900 mM. The fourth set of samples is highly turbid media containing optically inactive glycerol with the microsphere weight fraction kept constant at 2.75×10^{-3} (same scattering coefficient range as set 3). The glycerol concentrations are such that they yield the same solution refractive index as glucose in the third set of samples. This is used to make comparison measurements on the contributions to optical rotation due to chirality and due to refractive-index matching effects, in which the increase of glucose concentration reduces the refractive index difference between the scattering particles and the surrounding medium, resulting in the decrease of the scattering coefficient of the turbid medium.[8,22–24]

4 Results and Discussion

Figure 3 shows how optical rotation α, surviving linear polarization β_{linear}, and intensity I of the light emerging from turbid media (no glucose) change as a function of detection angle θ and turbidity of sample, indicated by scattering coefficient μ_s. The results of about 32 measurements are summarized in the figure. Somewhat surprisingly, Fig. 3(a) shows large optical rotations even in the absence of glucose, as suggested by previous initial observations.[3,15,18] As seen, the magnitude of α is a strong and complex function of both sample turbidity and detection angle. For lower turbidity ($\mu_s=20$ to 40 $\mathrm{cm^{-1}}$), α increases with θ from about 1° to about 4° and then decreases again for $\theta>130°$. For turbid media with $\mu_s=50$ to 80 $\mathrm{cm^{-1}}$, α displays a monotonic increase with θ from ~1 to 12°. For highly turbid media ($\mu_s=90$ to 100 $\mathrm{cm^{-1}}$), α exhibits oscillations at smaller detection angles and then increases monotonically from ~2 to 12° when $\theta>90°$. It is noticed that in these highly turbid samples, α is slightly nonzero even in the forward direction, possibly arising from minor detector misalignment about $\theta=0°$. Clearly then, multiple scattering significantly changes the orientation of the linear polarization plane, thus resulting in an apparent optical rotation in most directions. The magnitude of this change in linear polarization orientation depends strongly

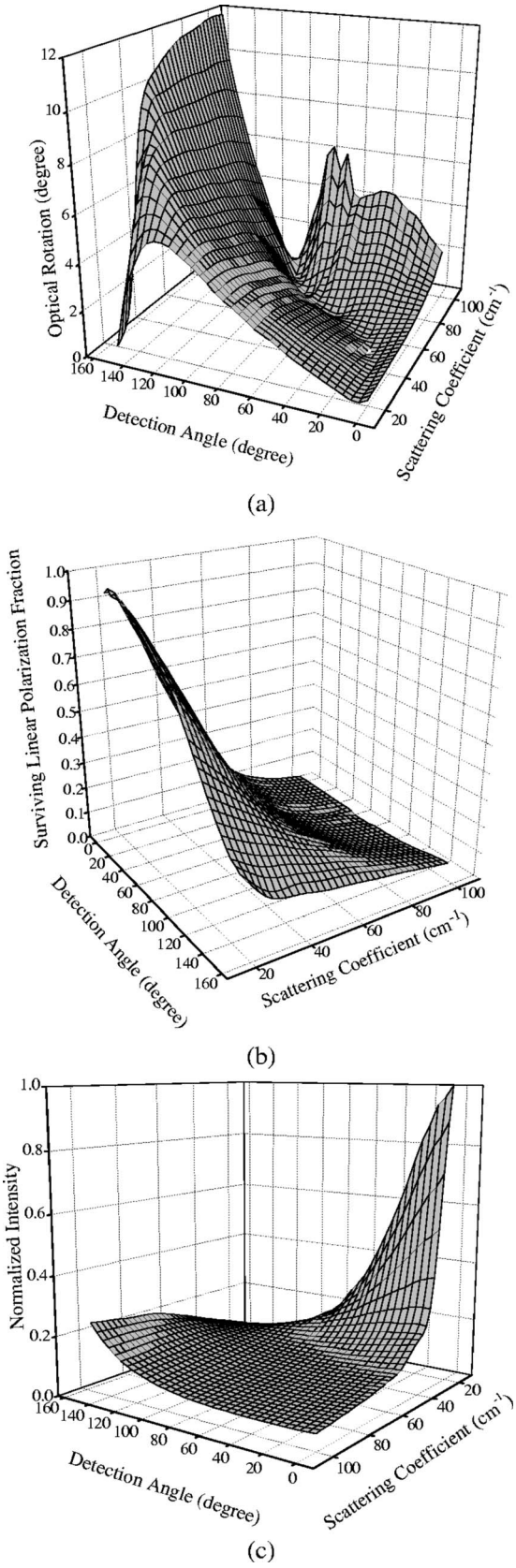

Fig. 3 Measured angular and turbidity dependence of polarization states of emerging light from turbid media in the absence of glucose (a) Optical rotation; (b) surviving linear polarization fraction; (c) normalized intensity. The orientation of the horizontal axes is different for the three plots to enable better visualization.

on both sample turbidity and detector orientation angle. Larger θ generally means larger change of the polarization plane orientation. Further studies are underway to interpret these trends. Regardless of the mechanism, the data unequivocally shows that optical rotation results in a turbid polarimetry setting must be interpreted with caution, in that α is not only caused by chirality of glucose molecules as is the case for clear-media glucometry.

Figure 3(b) shows that β_{linear} decreases significantly with increasing turbidity and detection angle for low and moderately turbid media. In the forward direction ($\theta=0°$), β_{linear} drops from 0.9 at $\mu_s=20$ cm^{-1} to 0.35 at $\mu_s=60$ cm^{-1}. For a turbid medium with $\mu_s=20$ cm^{-1}, β_{linear} drops from 0.9 at $\theta=0°$ to 0.2 at $\theta=155°$. With further increases of turbidity of the sample, β_{linear} still decreases but becomes less dependent on detection angle as its overall levels drop. The data suggests that for low and moderately turbid media, photons exiting at smaller angles may be scattered fewer times than the photons exiting at larger detection angles, yielding the smaller depolarization effects. With the increase of sample turbidity, photons encounter more scattering events on route to reaching the detector, resulting in greater depolarization. With further increase in sample turbidity, photons exiting in any direction encounter almost the same amount of scattering events, as suggested by the decreasing angular dependence of β_{linear}.

Figure 3(c) shows that the intensity I is not strongly dependent on the detection angle θ except for low turbidity media ($\mu_s\sim25$ cm^{-1}), where I drops from $\sim$0.9 to 0.1 when θ increases from 0 to 155°. For samples with $\mu_s>40$ cm^{-1}, the intensity is low and largely independent of detection angle, although exhibiting a minor increase for $\theta>90°$.

Selected subsets of the above experimental results were compared with polarization-sensitive Monte Carlo (MC) simulations developed in our group,[3,25] a validated model that expands upon the prior work of Kaplan et al.[26] and Jaillon et al.[27] In these simulations, the photons are propagated between scattering events, as determined by pseudorandom sampling of the scattering mean free path similar to conventional (intensity-only) MC models[28] of light propagation in tissue; the polarization information is tracked in the form of individual Stokes vectors, which are summed over a large number of tracked photon histories, to yield the experimentally observable macroscopic properties of interest. Optical activity due to the chiral nature of dissolved glucose is handled by imposing the rotation of the plane of linear polarization between the scattering events, using a Mueller matrix for a standard optical rotator.[3,25] The aim of the comparison is to validate the measurement results and predict the trends of polarization states of scattered light at $\theta>155°$, where measurements are not currently possible. Typical experiment-simulation comparison curves for glucose-free turbid suspensions are shown in Fig. 4. The MC simulations of the surviving linear polarization fraction as a function of detection angle [for $\mu_s=20$ cm^{-1}, Fig. 4(a)] and as a function of scattering coefficient [for $\theta=0°$, Fig. 4(b)] show similar trends to the experimental measurements, although further refinement may be necessary to improve agreement. The simulation in Fig. 4(a) predicts a significant increase of β_{linear} beyond 160°, a region currently unconfirmed with experimental measurements. This suggests the potential benefit of backward detection for highly turbid media, where surviving linear polarization fraction and signal intensity are relatively high. System modifications are underway to enable experimental validations at larger detection angles approaching the exact backscattering direction.

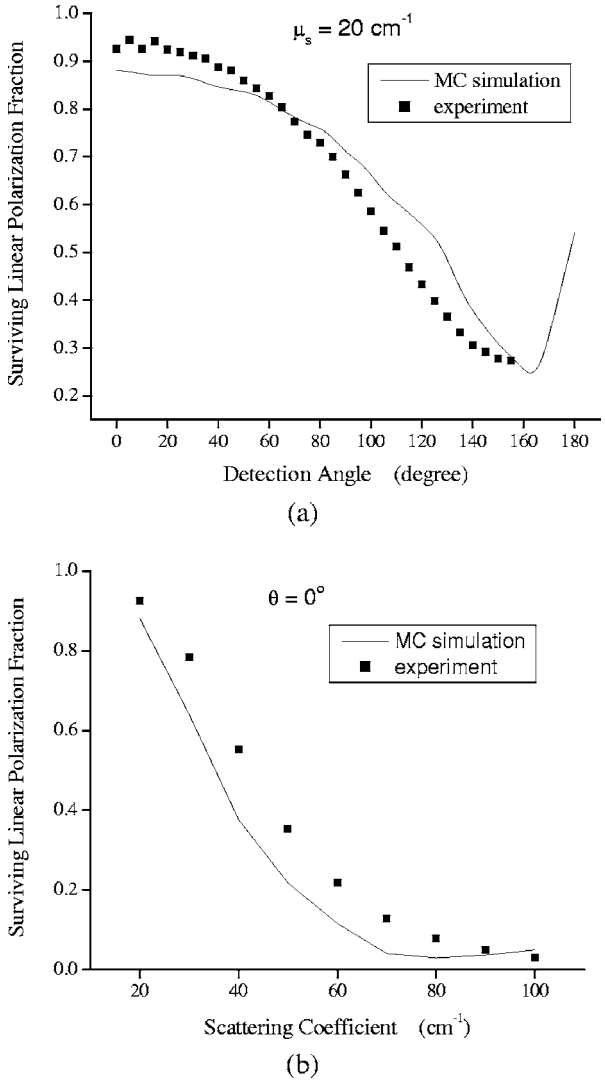

Fig. 4 Experimental data (squares) and MC simulations (line) for glucose-free turbid media in a cylindrical cuvette of 1 cm diameter. (a) Surviving linear polarization fraction as a function of detection angle for $\mu_s=20$ cm^{-1}; (b) surviving linear polarization fraction as a function of scattering coefficient at $\theta=0°$.

Figure 5 shows the effects of increasing glucose (20 to 900 mM) in moderately turbid media ($\mu_s=30$ cm^{-1} in glucose-free suspension) on polarization states of the emerging light detected at five different detection angles of $\theta=0$, 45, 90, 135, and 155°. Figure 5(a) shows that optical rotation decreases with glucose concentration at all detection angles except in the forward direction. The observed decrease in α may indicate that the optical rotation due to scattering and the optical rotation due to glucose chirality are in the opposite directions. If former is greater than the latter, addition of glucose can cause a decrease in the net apparent optical rotation. The optical rotation change detected at $\theta=155°$ is most sen-

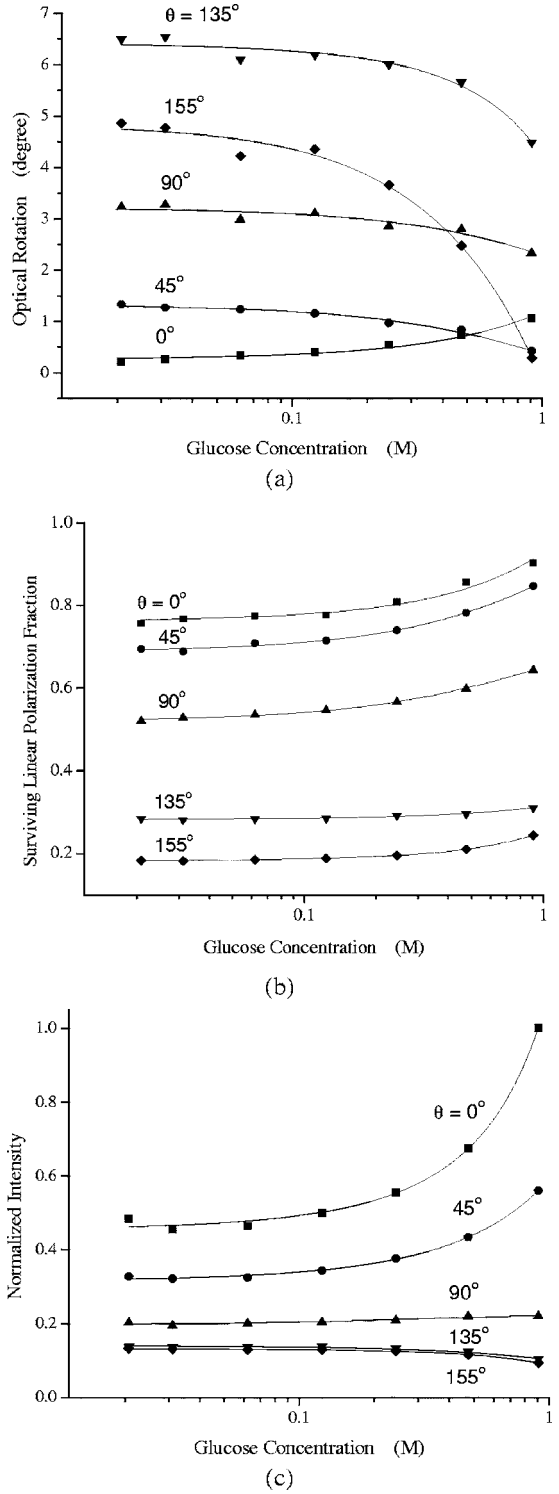

Fig. 5 Effects of glucose concentration (20 to 900 mM) in moderately turbid media (μ_s=30 cm^{-1} at 0 M glucose) on polarization states of emerging light detected at different detection geometries. (a) Optical rotation; (b) surviving linear polarization fraction; (c) normalized intensity. The symbols are data points; the lines are a guide for the eye.

sitive to glucose level change, yielding $\Delta\alpha \sim -4.5°$ for examined concentration change. Selecting a slightly different backward detection angle of $\theta=135°$ yields a $\Delta\alpha \sim -2.0°$ for the same glucose range. For comparison, the conventional detection geometry in the forward direction results in a much smaller $\Delta\alpha$ of $\sim +0.8°$. The data trends suggest that in the forward direction, glucose chirality is the main contributor to the observed optical activity; in other detection directions, the measured optical activity is dominated by scattering effects (as modulated by the addition of glucose, which (1) reduces scattering (2) is optically active). It is expected that there exists a detection angle at which the measured optical rotation has equal contributions from these reactive index matching and optical activity effects (as borne by the experimental results summarized in Fig. 7 below).

Figure 5(b) shows the change of corresponding surviving linear polarization fraction due to glucose for the same samples as in Fig. 5(a). β_{linear} increases with glucose concentration at all detection angles with $\Delta\beta \sim +0.15$ in forward direction and $\Delta\beta \sim +0.1$ at $\theta=155°$. This change is most likely due to the glucose refractive index matching, which effectively reduces the sample turbidity, thus decreasing the depolarizing effects of multiple scattering. Even through the backward detection displays a slightly reduced $\Delta\beta_{linear}$ and overall lower levels of surviving linear polarization, it is still an attractive detection geometry if both α and β_{linear} are used as metrics of glucose concentration.

Figure 5(c) shows the change of normalized intensity I in the presence of varying glucose amounts. As seen, the intensity is higher in the forward hemisphere, and glucose-induced changes are very much directions-dependent, being negligible for $\theta > 90°$ and most pronounced in the forward direction. These polarization-independent changes in detected light intensity with varying glucose levels most likely originate from the index-matching effect of glucose, which reduces sample scattering properties as previously outlined.

Figure 6 is analogous to Fig. 5 but displays the results for the case of higher scattering (μ_s=100 cm^{-1} in glucose-free suspension). Opposite to Fig. 5(a), the optical rotation α in Fig. 6(a) decreases with glucose concentration at a forward detection direction and increases with glucose concentration at larger detection angles (135 and 155°). The monotonically decreasing α in the forward direction indicates an overall dominance of the glucose refractive index matching effect that reduces scattering and the apparent optical rotation it causes in this high-scattering regime. The increase in α at larger angles implies that more complicated mechanisms are contributing to optical rotation. For example, the reduction in scattering due to glucose-induced refractive index matching effect can cause the observed increase in α at large scattering angles, by lengthening the effective pathlength over which the detected photons can accrue additional optical rotation. Figure 6(b) shows that β_{linear} levels and their sensitivity to glucose changes are different in their dependence on θ as compared with optical rotation. The magnitude and increase of β_{linear} caused by increasing glucose levels are both largest in backward directions. The intensity dependence of Fig. 6(c) shows that more photons escape the highly turbid medium in the backward hemisphere and the glucose-induced intensity reduction is the largest at $\theta=155°$.

Figure 7(a) displays the relative importance of scattering-induced and optical activity-induced glucose contributions to the observed optical rotation in moderately turbid samples. As θ is increased from 5 to 30° in samples with

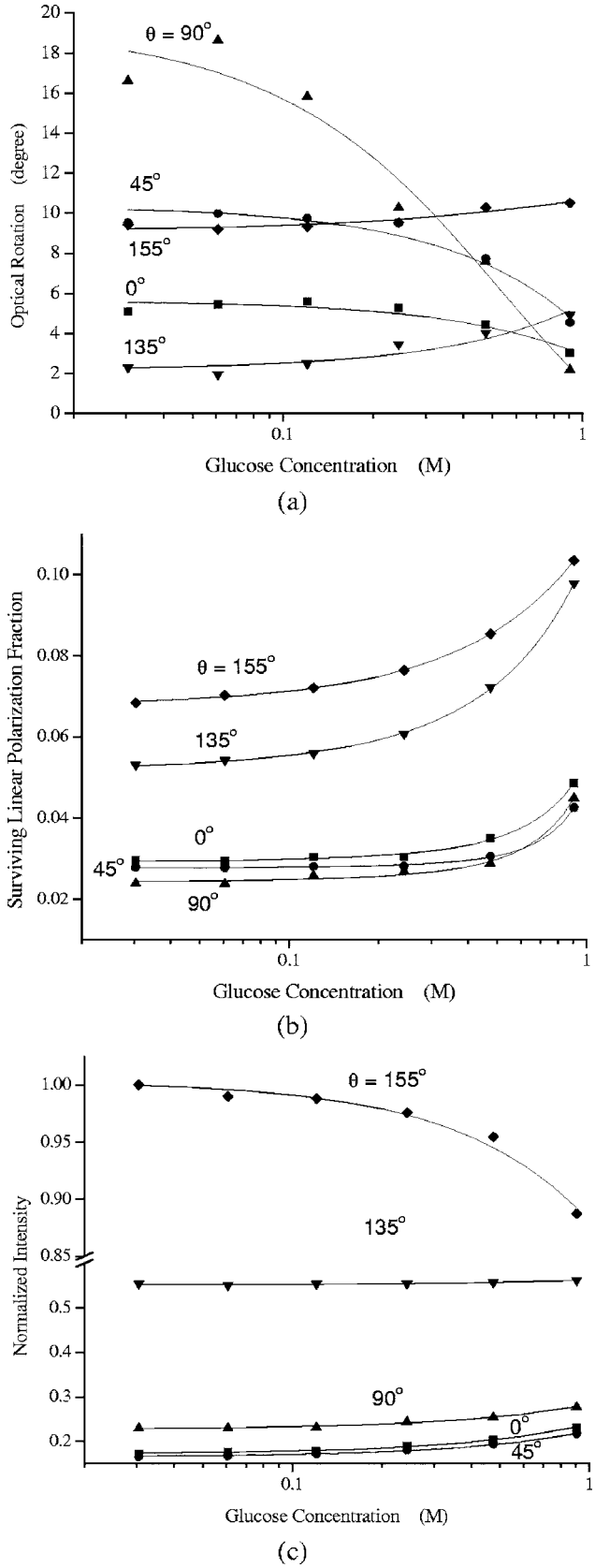

Fig. 6 Effects of glucose concentration (30 to 900 mM) in highly turbid media (μ_s=100 cm^{-1} at 0 M glucose) on polarization states of emerging light detected at different detection geometries. (a) Optical rotation; (b) surviving linear polarization fraction; (c) normalized intensity. The symbols are data points; the lines are a guide for the eye.

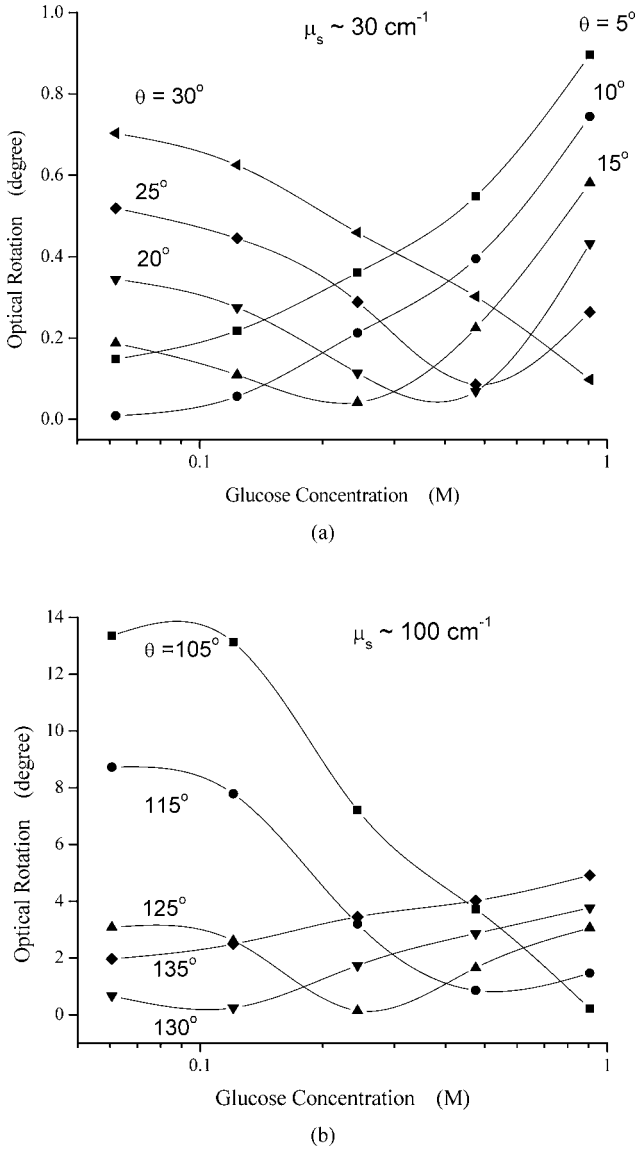

Fig. 7 Glucose effects on optical rotation in turbid media, in order to examine the chirality and refractive index matching contributions. (a) Moderately turbid media ($\mu_s \sim 30$ cm^{-1}); (b) highly turbid media ($\mu_s \sim 100$ cm^{-1}). The symbols are data points; the lines are a guide for the eye.

$\mu_s \sim 30$ cm^{-1}, two distinct regimes of optical rotation contribution are evident. Near the forward direction (θ=5 and 10°), increasing the glucose concentration leads to nearly monotonic increase in measured optical rotation. Conversely, for detection angles of 25 and 30°, a decrease in optical rotation is seen. We interpret the former behavior as being dominated by optical activity, whereas the latter is indicative of scattering effect dominance as engendered by glucose refractive index matching. The θ=15° detection geometry represents an intermediate case of roughly equal contributions, at least for this sample geometry and this scattering coefficient ($\mu_s \sim 30$ cm^{-1}). An analogous graph for higher scattering ($\mu_s \sim 100$ cm^{-1}) seen in Fig. 7(b) shows that the transition region occurs at much higher detection angles and also indicates overall higher optical rotation levels. It appears that α de-

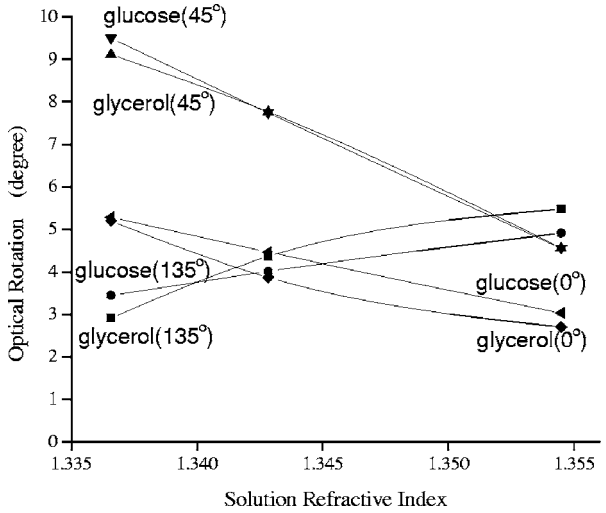

Fig. 8 Comparison measurements in highly turbid suspensions ($\mu_s \sim 100$ cm^{-1}) containing glycerol or glucose. For the same amount of refractive index change caused by both optically active glucose and optically inactive glycerol, similar amounts of optical rotation in both forward and backward detection geometries are seen. For the range of index matching values shown, the scattering coefficient changes from 98.3 cm^{-1} (n_{medium}=1.337) to 92.7 cm^{-1} (n_{medium}=1.355). The symbols are data points; the lines are a guide for the eye.

tected at θ=125° has roughly equal contributions from chirality and from index matching for the examined range of glucose concentration. Given the larger magnitude of the drop, we conclude that the refractive index matching effect is the stronger one in highly scattering media.

Glycerol comparison measurement results shown in Fig. 8 reveal that the same solution refractive index change (from 1.337 to 1.355) due to presence of optically active glucose (243 to 900 mM glucose concentration) and optically inactive glycerol (2.49 to 17.5%) yields similar amounts of optical rotation detected at θ=0, 45, and 135° in media with $\mu_s \sim 100$ cm^{-1}. This implies that the refractive index matching effect dominates over optical activity in its contribution to optical rotation in highly turbid media, as is also suggested by Fig. 7(b). A similar conclusion was reached by Hadley et al. for media with lower scattering.[29]

5 Summary

We have demonstrated that the polarization parameters α, β_{linear} and overall scattered intensity I, simultaneously obtained from polarimetric measurements in different detection directions around a scattering sample, depend in a varied and complex way on a number of factors, including sample glucose concentration. For example, in scattering media with μ_s in the 30 to 100 cm^{-1} range, large changes in α and β_{linear} were detected in the backward direction as glucose levels increased to ~1 M. The three parameters (α, β_{linear}, and I) form a potentially attractive three-channel probe for glucose level monitoring in turbid media, although their dependence on sample properties and experimental geometry is complicated. The weak dependence of the derived optical rotation on the chiral nature of glucose in multiply scattering samples, while surprising and disappointing initially, may actually remove some of the difficulties of polarimetry caused by other chiral confounders in biological tissues. The range of validity of the observed trends is currently being explored in other chiral scattering systems. Further research will focus on the optimal detection geometry for maximizing sensitivity to glucose concentration levels closer to the physiological level. Other alternative detection geometries, such as out-of-plane detection, are beginning to be explored.[30] Expanding upon the presented methodology, the effects of media absorption, linear birefringence, and the possibility of multiwavelength (spectroscopic) polarimetry coupled with chemometric analysis are also under investigation.

6 Conclusions

We have demonstrated the feasibility of studying the polarization states of scattered light from turbid media in different directions using a refined linear Stokes polarimeter. An extensive experimental study was performed, concentrating on sample (turbidity, chirality) and system (detection angle) variables. Selected validation with polarization-sensitive MC simulation model was performed. It is found that in turbid media, the scattering process itself can cause a large optical rotation, even in the absence of glucose. In general, the magnitude of the optical rotation is strongly dependent on sample turbidity, detection angle, and glucose levels. For example, in highly turbid media (μ_s=100 cm^{-1}), optical rotation can reach up to 20° levels and can exhibit large changes ($\Delta\alpha$ up to 10 to 15°) over the ~1 M glucose concentration range. The surviving linear polarization fraction decreases with increasing turbidity and also with the detection angle for low and moderately turbid media. Its angular dependence becomes less pronounced with increasing turbidity and, in fact, reverses for highly turbid samples. It is demonstrated that the three derived polarization parameters (α, β_{linear}, and I) depend on glucose levels, albeit in a complicated way. The sensitivity to glucose is strongly detection-angle–dependent, suggesting that the backward detection angles may be preferable for glucose sensing in highly turbid media, such as biological tissue, although the complicated angular and turbidity dependence of optical rotation α may make this metric less glucose-specific. Comparison measurements in turbid media containing (optically inactive) glycerol indicate that the optical rotation dependence on (optically active) glucose concentration is not due to its chiral nature, but is mainly caused by the refractive index matching effect.

Acknowledgments

The authors thank Dr. Theodore Oakberg (Hinds Instruments, Hillsboro, Oregon) for helpful discussions and the Natural Sciences and Engineering Research Council of Canada (NSERC) for financial support of this research.

References

1. J. A. Tamada, M. Lesho, and M. J. Tierney, "Keeping watch on glucose: new monitors help fight the long-term complication of diabetes," *IEEE Spectrum* **39**, 52–57 (2002).
2. A. J. Berger, "Minimally invasive technologies for optical glucose monitoring," *Opt. Photonics News* **12**, S8–S11 (2001).
3. D. Côté and I. A. Vitkin, "Balanced detection for low-noise precision polarimetric measurements of optically-active, multiply-scattering tissue phantoms," *J. Biomed. Opt.* **9**, 213–220 (2004).

4. O. S. Khalil, "Spectroscopic and clinical aspects of noninvasive glucose measurements," *Clin. Chem.* **45**, 165–177 (1999).
5. K. V. Larin, M. S. Eledrisi, M. Motamedi, and R. O. Esenaliev, "Noninvasive blood glucose monitoring with optical coherence tomography," *Diabetes Care* **25**, 2263–2267 (2002).
6. R. R. Ansari, S. Bockle, and L. Rovati, "New optical scheme for a polarimetric-based glucose sensor," *J. Biomed. Opt.* **9**, 103–115 (2004).
7. M. Kohl and M. Cope, "Influence of glucose concentration on light scattering in tissue-simulating phantoms," *Opt. Lett.* **19**, 2170–2172 (1994).
8. J. S. Maier, S. A. Walker, S. Fantini, M. A. Franceschini, and E. Gratton, "Possible correlation between blood glucose concentration and the reduced scattering coefficient of tissues in the near infrared," *Opt. Lett.* **19**, 2062–2064 (1994).
9. J. T. Bruulsema, J. E. Hayward, T. J. Farrell, M. S. Patterson, L. Heinemann, M. Berger, T. Koschinsky, J. Sandahl-Christiansen, H. Orskov, M. Essenpreis, G. Schmelzeisen-Redeker, and D. Böcker, "Correlation between blood glucose concentration in diabetics and noninvasively measured tissue optical scattering coefficient," *Opt. Lett.* **22**, 190–192 (1997).
10. R. J. McNichols and G. L. Coté, "Optical glucose sensing in biological fluids: an overview," *J. Biomed. Opt.* **5**, 5–16 (2000).
11. M. Mehrübeoğlu, N. Kehtarnavaz, S. Rastegar, and L. V. Wang, "Effect of molecular concentrations in tissue-simulating phantoms on images obtained using diffuse reflectance polarimetry," *Opt. Express* **3**, 286–297 (1998).
12. R. C. N. Studinski and I. A. Vitkin, "Methodology for examining polarized light interactions with tissues and tissuelike media in the exact backscattering direction," *J. Biomed. Opt.* **5**, 330–337 (2000).
13. M. P. Silverman, W. Strange, J. Badoz, and I. A. Vitkin, "Enhanced optical rotation and diminished depolarization in diffusive scattering from a chiral liquid," *Opt. Commun.* **132**, 410–416 (1996).
14. I. A. Vitkin, R. D. Lazslo, and C. L. Whyman, "Effects of molecular asymmetry of optically active molecules on the polarization properties of multiply scattered light," *Opt. Express* **10**, 222–229 (2002).
15. I. A. Vitkin and E. Hoskinson, "Polarization studies in multiply scattering chiral media," *Opt. Eng.* **39**, 353–362 (2000).
16. A. J. Hunt and D. R. Huffman, "A new polarization-modulated light scattering instrument," *Rev. Sci. Instrum.* **44**, 1753–1762 (1973).
17. P. S. Hauge, "Recent developments in instrumentation in ellipsometry," *Surf. Sci.* **96**, 108–140 (1980).
18. J. C. Kemp, G. D. Henson, C. T. Steiner, and E. R. Powell, "The optical polarization of the sun measured at a sensitivity of parts in 10 million," *Nature (London)* **326**, 270–273 (1987).
19. R. Anderson, "Measurement of Mueller Matrices," *Appl. Opt.* **31**, 11–13 (1992).
20. M. Diem, G. M. Roberts, O. Lee, and A. Barlow, "Design and performance of an optimized dispersive infrared dichrograph," *Appl. Spectrosc.* **42**, 20–27 (1988).
21. C. F. Bohren and D. R. Huffman, Appendix A in *Absorption and Scattering of Light by Small Particles*, John Wiley, New York (1983).
22. M. Tarumi, M. Shimada, T. Murakami, M. Tamura, M. Shimada, H. Arimoto, and Y. Yamada, "Simulation study of *in vitro* glucose measurement by NIR spectroscopy and a method of error reduction," *Phys. Med. Biol.* **48**, 2373–2390 (2003).
23. H. Liu, B. Beauvoit, M. Kimura, and B. Chance, "Dependence of tissue optical properties on solute-induced changes in refractive index and osmolarity," *J. Biomed. Opt.* **1**, 200–211 (1996).
24. J. Y. Qu and B. C. Wilson, "Monte Carlo modeling studies of the effect of physiological factors and other analytes on the determination of glucose concentration *in vivo* by near infrared optical absorption and scattering measurements," *J. Biomed. Opt.* **2**, 319–325 (1997).
25. D. Côté and I. A. Vitkin, "Robust concentration determination of optically active molecules in turbid media with validated three-dimensional polarization sensitive Monte Carlo calculations," *Opt. Express* **13**, 148–163 (2005).
26. B. Kaplan, G. Ledanois, and B. Drévillon, "Muller Matrix of dense polystyrene latex sphere suspensions: measurements and Monte Carlo simulation," *Appl. Opt.* **40**, 2769–2777 (2001).
27. F. Jaillon and H. Saint-Jalmes, "Description and time reduction of a Monte Carlo code to simulate propagation of polarized light through scattering media," *Appl. Opt.* **42**, 3290–3296 (2003).
28. L. Wang, S. L. Jacques, and L. Zheng, "MCML-Monte Carlo modeling of light transport in multi-layered tissues," *Comput. Methods Programs Biomed.* **47**, 131–146 (1995).
29. K. C. Hadley and I. A. Vitkin, "Optical rotation and linear and circular depolarization rates in diffusively scattered light from chiral, racemic and achiral turbid media," *J. Biomed. Opt.* **7**, 291–299 (2002).
30. X. Guo, M., F. G. Wood, and I. A. Vitkin, "Effects of detection geometry on polarimetric measurements of scattered light from turbid media containing optically active glucose molecules," *Proc. SPIE* **5969**, 59691K (2005).